Thermoelectric effect in a superconductor with Bogoliubov Fermi surfaces

Tomoya Sano,[1] Takumi Sato,[1,2] Akihiro Sasaki,[1] Satoshi Ikegaya,[3,4] Shingo Kobayashi,[5] and Yasuhiro Asano[1]
[1]*Department of Applied Physics, Hokkaido University, Sapporo 060-8628, Japan*
[2]*Graduate School of Science, Hokkaido University, Sapporo 060-0810, Japan*
[3]*Department of Applied Physics, Nagoya University, Nagoya 464-8603, Japan*
[4]*Institute for Advanced Research, Nagoya University, Nagoya 464-8601, Japan*
[5]*RIKEN Center for Emergent Matter Science, Wako, Saitama 351-0198, Japan*

(Received 15 November 2024; revised 12 March 2025; accepted 16 April 2025; published 1 May 2025)

We study theoretically the thermoelectric effect in a superconducting state having the Bogoliubov-Fermi surfaces which stays in a thin superconducting layer between a conventional superconductor and an insulator. The thermoelectric coefficients calculated based on the linear response theory show the remarkable anisotropy in real space, which are explained well by the anisotropic shape of the Bogoliubov-Fermi surface in momentum space. Our results indicate a way to check the existence of the Bogoliubov-Fermi surfaces in a stable superconducting state because the anisotropy is controlled by the direction of an applied magnetic field.

DOI: 10.1103/PhysRevB.111.174503

I. INTRODUCTION

In a superconductor belonging to unconventional symmetry class such as d-wave and p-wave, a Bogoliubov quasiparticle at zero energy (Fermi level) exists only at nodes of the pair potential. This conclusion is valid when the superconducting states are described effectively by the 2×2 Bogoliubov-de Gennes (BdG) Hamiltonian. When an electron has internal degrees of freedom, such as spin and sublattice, the size of the BdG Hamiltonian becomes as large as 4×4 or more. A Bogoliubov quasiparticle in such superconducting states can form Fermi surfaces called Bogoliubov-Fermi surfaces (BFSs) [1–3]. Therefore, multiband superconductors, $j = 3/2$ superconductors, and usual $s = 1/2$ superconductors with spin-dependent potentials can have the BFSs in their superconducting states [3–15].

The residual finite density of states (DOS) at zero energy is a direct consequence of the BFSs, which can be observed by using spectroscopies on a surface [16,17] and modifies the bulk properties such as specific heat [11,18,19], magnetic properties, and transport properties [20–23]. However, it is difficult to catch convincing evidences of the BFSs because the residual density of states is derived also from random impurities. Theoretical studies have suggested to catch signatures of the BFSs through transport properties in a normal-metal/superconductor junction [11,14,18,19,24–27]. It should be noted that superconducting states having BFSs are thermodynamically unstable as pointed out by numerical simulations for $j = 3/2$ superconductors [9,28]. The instability is partially derived from a fact that quasiparticles on the BFSs coexist with odd-frequency Cooper pairs [29–31]. A possibility of an odd-frequency superconductivity has been discussed as a result of Cooper pairing of two quasiparticles on the BFSs [32]. In order to establish the physics of quasiparticles on the BFSs, it is necessary to realize stable superconducting states with BFSs and clarify their specific phenomena. In what follows, we address these issues.

In this paper, we theoretically discuss the thermoelectric effect due to the quasiparticle on the BFSs. The electric current $\boldsymbol{j}$ flows in the presence of the spatial gradient of a temperature ∇T. In the relation $\boldsymbol{j} = -\alpha \nabla T$, the thermoelectric coefficient α represents the strength of the effect. The thermoelectric coefficient in a uniform of superconductor α_{S} has been formulated in terms of the solutions of the transport equation [33,34] and the quasiclassical Green's functions [35]. The expression at low temperatures $\alpha_{\mathrm{S}} \approx \alpha_{\mathrm{N}} \exp(-\Delta/T)$ suggests that the thermoelectric coefficient of a conventional superconductor is exponentially smaller than that in the normal state α_{N}. The results can be explained well by the absence of the DOS around zero energy due to the pair potential Δ. We discuss the effects of a quasiparticle on the BFSs on the thermoelectric effect in a stable superconducting state at a semiconductor thin film as illustrated in Fig. 1. The BFSs appear at the film in the presence of both spin-orbit interactions (SOI) and strong magnetic fields [4,7,15]. The thermoelectric coefficient is calculated based on the linear response theory by using the Keldysh Green's function method. The calculated results show that the thermoelectric effect is anisotropic in real space, which reflects the anisotropic shape of the BFSs in momentum space. Moreover, the thermoelectric coefficient in the presence of the BFSs can be larger than its normal state value. The enhancement in the thermoelectric effect is explained by the shift of the gapped DOS due to a magnetic field. We conclude that the existence of the BFSs can be directly confirmed by the anisotropy of the thermoelectric coefficient.

This paper is organized as follows. In Sec. II, we describe the realization of BFSs in the semiconductor-superconductor hybrid system. In Sec. III, we derive the thermoelectric coefficient within the linear response to the spatial gradient of temperature. In Sec. IV, the calculated results of the DOS and those of the thermoelectric coefficients are presented. We discuss the meaning of the obtained results in Sec. V. The conclusion is given in Sec. VI.

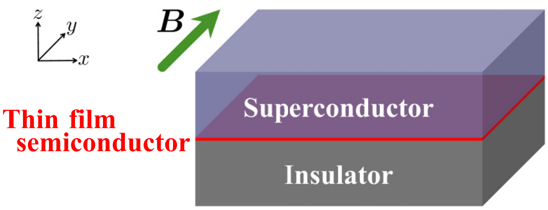

FIG. 1. Schematics of a proximity structure considered in this paper. We focus on two-dimensional electronic states at a thin semiconductor sandwiched between a superconductor and an insulator. Because of inversion symmetry breaking in the z direction, Rashba spin-orbit interaction works for electrons. In the presence of an external magnetic field applied in the y direction and the proximity-effect induced pair potential, a superconducting state with Bogoliubov-Fermi surfaces can be realized in the thin film.

II. MODEL

We discuss the thermoelectric effect in two-dimensional electronic states realized in a thin semiconductor sandwiched by a spin-singlet s-wave superconductor and an insulator under an in-plane magnetic field as illustrated in Fig. 1. The BdG Hamiltonian in a thin semiconductor [7,15] reads

$$\check{H}_{\rm BdG} = \begin{bmatrix} \hat{h}_{\rm N}(\boldsymbol{k}) & \Delta i\hat{\sigma}_y \\ -\Delta i\hat{\sigma}_y & -\hat{h}^*_{\rm N}(-\boldsymbol{k}) \end{bmatrix}, \tag{1}$$

$$\hat{h}_{\rm N}(\boldsymbol{k}) = \xi_{\boldsymbol{k}}\hat{\sigma}_0 - \boldsymbol{V}\cdot\hat{\boldsymbol{\sigma}} - \boldsymbol{\lambda}\times\boldsymbol{k}\cdot\hat{\boldsymbol{\sigma}}, \tag{2}$$

$$\xi_{\boldsymbol{k}} = \hbar^2\boldsymbol{k}^2/(2m) - \mu, \quad \boldsymbol{V} = (0, V, 0), \tag{3}$$

with $V = \frac{1}{2}g\mu_B B$, where μ is the chemical potential, B is the amplitude of an external magnetic field in the y direction, g is the g-factor, and μ_B is the Bohr magneton. The Pauli's matrices in spin space are denoted by $\hat{\boldsymbol{\sigma}} = (\hat{\sigma}_x, \hat{\sigma}_y, \hat{\sigma}_z)$ and $\hat{\sigma}_0$ is the unit matrix in spin space. The pair potential at the thin film is Δ. The vector $\boldsymbol{\lambda}$ is parallel to the z direction because inversion symmetry is broken along the z direction in the proximity structure. In such a situation, a Zeeman field in the xy plane enables the Bogoliubov-Fermi surfaces [4,7,15,25]. The reasons why we need to consider such a junction are explained below.

It is widely accepted that spin-singlet superconductivity is fragile in strong Zeeman potential V. However, to realize the BFSs in a conventional superconductor [4,7], the amplitude of a Zeeman field must be larger than the Clogston-Chandrasekhar limit [36,37]. Here, we assume that the pair potential Δ is induced in a thin semiconductor due to the proximity effect from a parent superconductor. In such a system, induced pair potential would be smaller than that of the parent superconductor $\Delta_{\rm bulk}$. In addition, it would be possible to choose a semiconductor with a large g-factor ($g > 2$) [38–42], which enables a larger Zeeman potential in a semiconductor V than that in the bulk of superconductor $V_{\rm bulk}$. For example, $g \sim 10$ or larger was reported in a two dimensional Al-InAs hybrid system [38–41]. A condition for the appearance of the BFSs in a thin semiconductor

$$\Delta < V = \tfrac{1}{2}g\mu_B B, \tag{4}$$

and that for the stable superconducting state in the bulk

$$\Delta_{\rm bulk} \gg V_{\rm bulk} \sim \mu_B B, \tag{5}$$

can be satisfied simultaneously in the proximity structure in Fig. 1. In what follows, we also assume that the transition to the superconducting phase is always the second-order [31] and that the dependence of Δ on temperatures is described by BCS theory.

In a junction shown in Fig. 1, the thermoelectric current flows only in the semiconducting segment. The electric current is absent in an insulator. Furthermore, the thermoelectric coefficient in the parent superconductor $\alpha_{\rm S} \approx \alpha_{\rm N}\exp(-\Delta_{\rm bulk}/T) \ll \alpha_{\rm N}$ is almost zero at low temperatures [34] with $\alpha_{\rm N}$ being the thermoelectric coefficient in the normal state. Therefore, the electric current flowing through the semiconducting film dominates the thermoelectric effect of the whole structure in Fig. 1.

III. CURRENT FORMULA

The electric current in the weak coupling limit [35] is represented by

$$\boldsymbol{j}(\boldsymbol{R}) = \frac{e}{4}\int \frac{d\boldsymbol{k}d\epsilon}{(2\pi)^{d+1}} i\boldsymbol{v}{\rm Tr}[\check{G}^K(\boldsymbol{R},\boldsymbol{k},\epsilon)], \tag{6}$$

with $\boldsymbol{v} = \hbar\boldsymbol{k}/m$ and $\boldsymbol{R}$ being the velocity and the place in real space, respectively. The Keldysh Green's function $\check{G}^K$ is the solution of the Gor'kov equation,

$$\left[\begin{pmatrix} \check{L}_0 + \check{L}_1 & 0 \\ 0 & \check{L}_0 + \check{L}_1 \end{pmatrix} - \begin{pmatrix} \check{\Sigma}^R & \check{\Sigma}^K \\ 0 & \check{\Sigma}^A \end{pmatrix}\right]_{(\boldsymbol{k},\epsilon)} \times \begin{bmatrix} \check{G}^R & \check{G}^K \\ 0 & \check{G}^A \end{bmatrix}_{(\boldsymbol{R},\boldsymbol{k},\epsilon)} = \begin{bmatrix} \check{1} & 0 \\ 0 & \check{1} \end{bmatrix}, \tag{7}$$

where

$$\check{L}_0(\boldsymbol{k},\epsilon) = \epsilon - \xi_{\boldsymbol{k}}\check{\tau}_3 - \check{V}, \tag{8}$$

$$\check{L}_1(\boldsymbol{k},\epsilon) = \frac{i}{2}\hbar\boldsymbol{v}\cdot\nabla_{\boldsymbol{R}}\check{\tau}_3, \tag{9}$$

$$\check{\Sigma}^X = \check{\Delta} - \check{\Sigma}^X_{\rm imp}, \tag{10}$$

with

$$\check{\Delta} = \begin{bmatrix} 0 & \hat{\Delta}(\boldsymbol{k}) \\ -\underset{\sim}{\hat{\Delta}}(\boldsymbol{k}) & 0 \end{bmatrix}, \tag{11}$$

$$\check{V} = \begin{bmatrix} \boldsymbol{V}\cdot\hat{\boldsymbol{\sigma}} + \boldsymbol{\lambda}\times\boldsymbol{k}\cdot\hat{\boldsymbol{\sigma}} & 0 \\ 0 & -\boldsymbol{V}\cdot\hat{\boldsymbol{\sigma}}^* + \boldsymbol{\lambda}\times\boldsymbol{k}\cdot\hat{\boldsymbol{\sigma}}^* \end{bmatrix}. \tag{12}$$

Here $\check{\tau}_i (i = 1, 2, 3)$ are Pauli's matrix in particle-hole space. The relation $\underset{\sim}{Y}(\boldsymbol{k},\epsilon) \equiv Y^*(-\boldsymbol{k},-\epsilon)$ represents particle-hole transformation of a function $Y(\boldsymbol{k},\epsilon)$. The self-energy due to random impurity scatterings is denoted by $\check{\Sigma}^X_{\rm imp}$. The details of the derivation are given in Appendix A.

The thermoelectric coefficient is calculated within the linear response to the thermal gradient which is considered through the distribution function

$$\Phi(\epsilon,\boldsymbol{R}) = \tanh\left[\frac{\epsilon}{2T(\boldsymbol{R})}\right]. \tag{13}$$

As discussed in Appendix A, the Green's function $\check{G}^{R,A}$ remains unchanged from its expression in equilibrium $\check{G}^{R,A}_0$

within the first order of $\nabla\Phi$. The Gor'kov equation for the Keldysh component becomes

$$\left[\check{L}_0(\boldsymbol{k},\epsilon)-\check{\Sigma}^R(\boldsymbol{k},\epsilon)+\frac{i}{2}\hbar\boldsymbol{v}\cdot\nabla_{\boldsymbol{R}}\check{\tau}_3\right]\check{G}^K(\boldsymbol{R},\boldsymbol{k},\epsilon)-\check{\Sigma}^K(\boldsymbol{k},\epsilon)\check{G}^A_0(\boldsymbol{k},\epsilon)=0. \quad (14)$$

We seek the solution of the Keldysh Green's function of the form $\check{G}^K=\check{G}^K_0+\delta\check{G}^K$ with Eqs. (A20) and (A21), where the first term is the solution in equilibrium and the second term is the deviation from it. In the limit of weak impurity scatterings, the solution within the first order of $\nabla\Phi$ is given by

$$\delta\check{G}^K=-\frac{i}{2}\hbar\boldsymbol{v}\cdot\nabla_{\boldsymbol{R}}\Phi(\epsilon,\boldsymbol{R})\times\left[\check{G}^R_0(\boldsymbol{k},\epsilon)\check{\tau}_3\left\{\check{G}^R_0(\boldsymbol{k},\epsilon)-\check{G}^A_0(\boldsymbol{k},\epsilon)\right\}\right]. \quad (15)$$

The current density and the thermoelectric coefficient are calculated as

$$\boldsymbol{j}^\mu(\boldsymbol{R})=-\alpha^{\mu,\nu}\nabla^\nu_{\boldsymbol{R}}T, \quad (16)$$

where μ and ν represent the direction of the current and the temperature gradient. Equation (A25) shows the general expression of the coefficient. Since all the off-diagonal elements of the coefficients are zero in a superconductor under consideration, we show only the diagonal elements as

$$\alpha^\nu=\frac{e\hbar}{32\pi T^2}\int_{-\infty}^{\infty}d\epsilon\frac{\epsilon}{\cosh^2(\epsilon/2T)}\times\int\frac{d\hat{\boldsymbol{k}}}{2\pi}(\hat{k}^\nu)^2\int_{-\infty}^{\infty}d\xi N(\xi)v^2(\xi)I(\boldsymbol{k},\epsilon), \quad (17)$$

$$I(\boldsymbol{k},\epsilon)=\mathrm{Tr}[\hat{G}(\hat{G}-\hat{G}^\dagger)-\underset{\sim}{\hat{G}}(\underset{\sim}{\hat{G}}-\underset{\sim}{\hat{G}}^\dagger)+\hat{F}\hat{F}^\dagger-\underset{\sim}{\hat{F}}\underset{\sim}{\hat{F}}^\dagger]^R_{(\boldsymbol{k},\epsilon)}, \quad (18)$$

with $\nu=x$ or y, where R in the superscript of Eq. (18) means that all the Green's functions belong to the retarded causality. Hereafter we omit "0" from the subscript of the Green's functions because the coefficient is expressed only by the Green's functions in equilibrium. We have used a relation

$$\frac{1}{V_{\mathrm{vol}}}\sum_{\boldsymbol{k}}\to\int\frac{d\hat{\boldsymbol{k}}}{2\pi}\int_{-\infty}^{\infty}d\xi\,N(\xi), \quad (19)$$

with $\hat{\boldsymbol{k}}=(k_x,k_y)/|\boldsymbol{k}|$. The 2×2 retarded Green's functions in Eq. (18) are the solution of the Gor'kov equation,

$$[\epsilon+i\delta-\check{H}_{\mathrm{BdG}}]\begin{bmatrix}\hat{G} & \hat{F}\\ -\underset{\sim}{\hat{F}} & -\underset{\sim}{\hat{G}}\end{bmatrix}^R_{(\boldsymbol{k},\epsilon)}=\check{1}. \quad (20)$$

Here we introduce the lifetime $\tau=\hbar/\delta$ of superconducting states. The Green's functions for the BdG Hamiltonian in Eq. (1) are calculated to be

$$\hat{G}(\boldsymbol{k},\epsilon)=\frac{1}{Z}[(\epsilon-\xi_{\boldsymbol{k}})\underset{\sim}{Z}_{\mathrm{N}}-(\epsilon+\xi_{\boldsymbol{k}})\Delta^2-\boldsymbol{V}\cdot\hat{\boldsymbol{\sigma}}(\underset{\sim}{Z}_{\mathrm{N}}+\Delta^2)-\boldsymbol{\alpha}_{\boldsymbol{k}}\cdot\hat{\boldsymbol{\sigma}}(\underset{\sim}{Z}_{\mathrm{N}}-\Delta^2)], \quad (21)$$

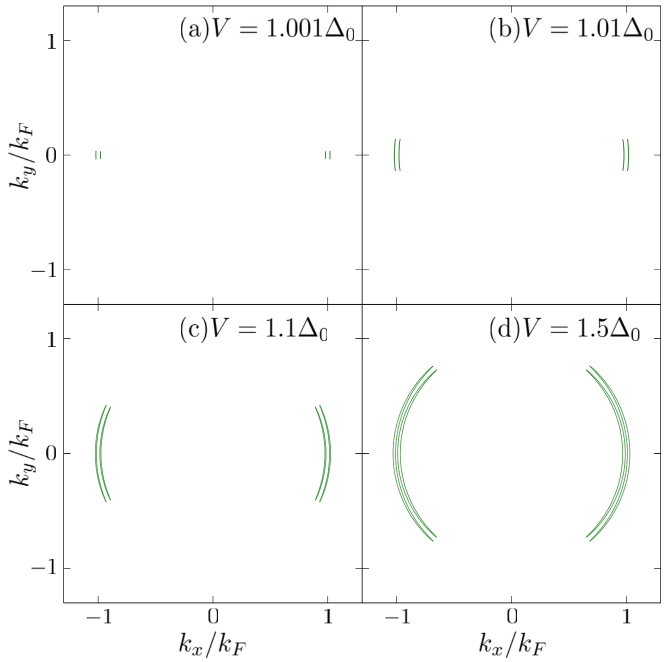

FIG. 2. The BFSs for $V=1.001\Delta_0$, $V=1.01\Delta_0$, $V=1.1\Delta_0$, and $V=1.5\Delta_0$ are displayed in (a), (b), (c), and (d), respectively. The strength of the Rashba SOI is fixed at $\lambda k_F=2\Delta_0$.

$$\hat{F}(\boldsymbol{k},\epsilon)=\frac{1}{Z}\left[\left(\epsilon^2-\xi_{\boldsymbol{k}}^2-\Delta^2-\boldsymbol{\alpha}_{\boldsymbol{k}}^2+\boldsymbol{V}^2\right)-2\epsilon\boldsymbol{V}\cdot\hat{\boldsymbol{\sigma}}-2\xi_{\boldsymbol{k}}\boldsymbol{\alpha}_{\boldsymbol{k}}\cdot\hat{\boldsymbol{\sigma}}-2i\boldsymbol{V}\times\boldsymbol{\alpha}_{\boldsymbol{k}}\cdot\hat{\boldsymbol{\sigma}}\right]\Delta i\hat{\sigma}_y, \quad (22)$$

$$Z=\left(\epsilon^2-\xi_{\boldsymbol{k}}^2-\Delta^2-\boldsymbol{\alpha}_{\boldsymbol{k}}^2+\boldsymbol{V}^2\right)^2+4(\boldsymbol{V}\times\boldsymbol{\alpha}_{\boldsymbol{k}})^2-4(\epsilon\,\boldsymbol{V}+\xi_{\boldsymbol{k}}\boldsymbol{\alpha}_{\boldsymbol{k}})^2, \quad (23)$$

$$\underset{\sim}{Z}_{\mathrm{N}}=(\epsilon+\xi_{\boldsymbol{k}})^2-(\boldsymbol{V}-\boldsymbol{\alpha}_{\boldsymbol{k}})^2,\quad \boldsymbol{\alpha}_{\boldsymbol{k}}=\boldsymbol{\lambda}\times\boldsymbol{k}. \quad (24)$$

The density of states per volume are calculated as

$$N(E)=\int\frac{d\hat{\boldsymbol{k}}}{2\pi}n(\hat{\boldsymbol{k}},E), \quad (25)$$

$$n(\hat{\boldsymbol{k}},E)=\frac{-N_0}{8\pi i}\int_{-\infty}^{\infty}d\xi\,\mathrm{Tr}[\hat{G}-\hat{G}^\dagger-\underset{\sim}{\hat{G}}+\underset{\sim}{\hat{G}}^\dagger]^R_{(\boldsymbol{k},E)}, \quad (26)$$

where $n(\hat{\boldsymbol{k}},E)$ is the angle-resolved density of states and N_0 is the DOS per volume in the normal states at the Fermi level.

For numerical simulation, we put $\delta=10^{-4}\Delta_0$ and $\Delta_0=0.02\mu$, where Δ_0 is the amplitude of induced pair potential at zero temperature.

IV. RESULTS

A. Density of states

In Fig. 2, we plot the BFSs (possible wave number for zero-energy eigenvalue) for several choices of Zeeman potentials $V=\frac{1}{2}g\mu_B B$. The size of the BFSs increases with the increase of V. For Zeeman potentials slightly larger than Δ_0 in Figs. 2(a) and 2(b), the quasiparticle states at zero energy

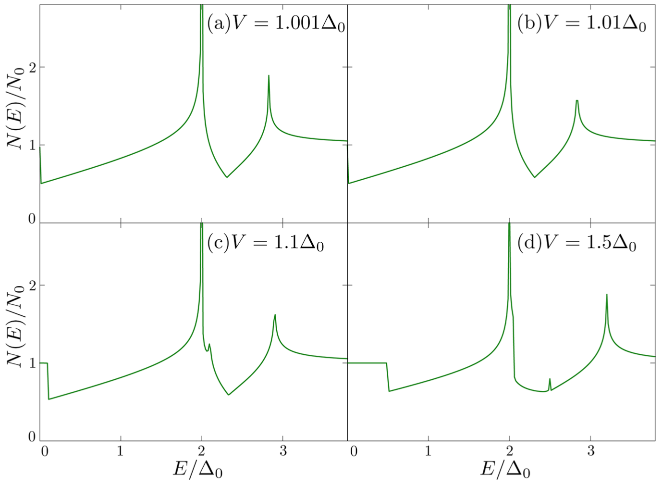

FIG. 3. Density of states calculated for several Zeeman potentials at $\lambda k_F = 2\Delta_0$.

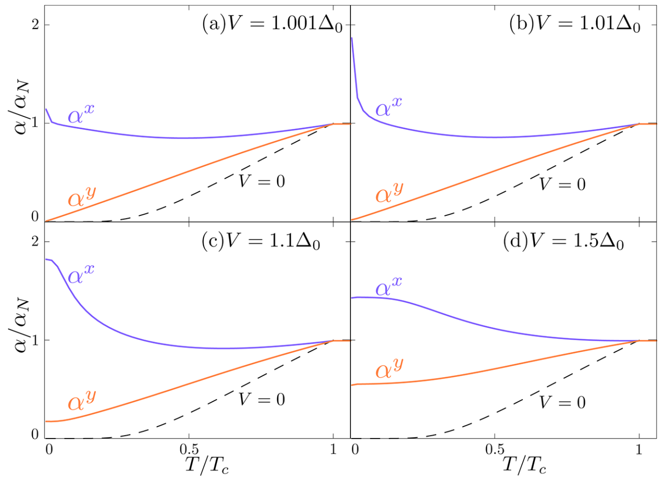

FIG. 4. The thermoelectric coefficient versus temperature. The coefficients in the two directions are shown with α^x and α^y. The broken lines show the results in the absence of a Zeeman potential.

are present around $\boldsymbol{k} = (k_x, k_y) = (\pm k_F, 0)$ and absent around $\boldsymbol{k} = (0, \pm k_F)$. The anisotropy of the BFSs is derived from the anisotropy in the normal states described by Eq. (2). For $\boldsymbol{V} = 0$ and $\boldsymbol{\lambda} = 0$, the original Fermi surface given by $k_x^2 + k_y^2 = k_F^2$ has a circular shape in momentum space. The isotropy of the Fermi surface is preserved for $\boldsymbol{V} \neq 0$ and $\boldsymbol{\lambda} = 0$ because the direction of a Zeeman field does not couple to any directions in the momentum space. A Zeeman field splits the doubly degenerate Fermi surface into two. The isotropy is preserved also for $\boldsymbol{V} = 0$ and $\boldsymbol{\lambda} \neq 0$ because the Rashba SOI preserves rotation symmetry along z axis. The Rashba SOI also splits the doubly degenerate Fermi surface into two. In the presence of the two interactions simultaneously $\boldsymbol{V} \neq 0$ and $\boldsymbol{\lambda} \neq 0$, the SOI couples momentum space to spin space and a Zeeman field specifies a special direction in momentum space. Thus, the anisotropy in the Fermi surface in the normal state is a result of the coexistence of the Rashba SOI and the Zeeman field. The BFSs in Fig. 2 inherit such the anisotropy even in the superconducting state. The BFSs always appear in the directions perpendicular to a Zeeman field $\boldsymbol{V}$. The results in Fig. 2 show the BFSs around $\boldsymbol{k} = (k_x, k_y) \approx (\pm k_F, 0)$ because a Zeeman field is applied in the y direction. The anisotropy of the BFSs is a source of the anisotropy in the thermoelectric effect.

In Fig. 2, the strength of the Rashba SOI is fixed at $\lambda k_F = 2\Delta_0$. Changing the amplitude of λ shifts the place of the BFSs only slightly in momentum space. We choose $\lambda k_F = 2\Delta_0$ throughout this paper because the characteristic features of the BFSs shown in Fig. 2 are insensitive to the choice of λ. A role of SOI in the formation of BFSs are discussed in Appendix B.

In Fig. 3, we present the DOS in the presence of the BFSs for several Zeeman potentials. The DOS at zero energy remains a finite value for all the Zeeman potentials. At $V = 0$, the DOS has two coherence peaks at $E = \pm\Delta$. Zeeman potentials shift these peaks depending on spin of an electron, which explains multiple peaks in $E/\Delta_0 = 2$ in Fig. 3. As Zeeman potentials increase, the width of a plateau near zero energy increases. This makes a superconducting phase with the BFSs unstable thermodynamically. To gain the condensation energy, the gapped energy spectra in DOS are necessary. The two-dimensional superconducting states with the BFSs are stabilized by the superconducting condensate in the parent superconductor.

B. Thermoelectric effect

The calculated results of the thermoelectric coefficients in the presence of the BFSs are plotted as a function of temperature for several of Zeeman potentials in Fig. 4, where the dependence of Δ on temperatures is described by BCS theory. The vertical axis is normalized to the coefficient in the normal state α_{N} which is isotropic in real space. The results in the absence of a Zeeman potential are shown with a broken line for comparison and obey $\alpha \approx \alpha_{\mathrm{N}} \exp(-\Delta/T)$ at low temperatures. Solid lines represent $\alpha^{x(y)}$ in which the electric current is perpendicular to magnetic field $\boldsymbol{j} \perp \boldsymbol{B}$(parallel to magnetic field $\boldsymbol{j} \parallel \boldsymbol{B}$). The thermoelectric coefficients indicate two characteristic features: the remarkable anisotropy in real space and $\alpha^x > \alpha_{\mathrm{N}}$. The anisotropy in the thermoelectric effect originates from the anisotropy of the BFSs in momentum space shown in Fig. 2. The zero-energy states around $\boldsymbol{k} = (\pm k_F, 0)$ in Fig. 2 can carry the electric current in the x direction. However, zero-energy states are absent around $\boldsymbol{k} = (0, \pm k_F)$, which results in the monotonic decrease of α^y with decreasing temperatures in Fig. 4. Such anisotropy is absent in a d-wave superconductor with the BFSs (see Appendix C for details).

To understand the unusual dependence of α^x on temperature, we analyze the angle-resolved DOS displayed in Fig. 5, where $n(\hat{\boldsymbol{k}}, E)$ along the k_x axis is shown by fixing k_y at 0. The angle-resolved DOS has two peaks for $E > 0$ because a Zeeman potential shifts the coherence peaks depending on spins of a quasiparticle. For $V \approx \Delta$ in Figs. 5(a) and 5(b), a peak appears almost zero energy in the angle-resolved DOS. A quasiparticle at such zero-energy states carries the thermoelectric current in the x direction. The relation $\alpha^x > \alpha_{\mathrm{N}}$ is a result of the shift of the coherence peak by a Zeeman potential. The DOS along the k_y axis calculated with putting $k_x = 0$ is shown in Fig. 6. In contrast to Fig. 5, the angle resolved DOS always has the gapped energy spectra at zero energy

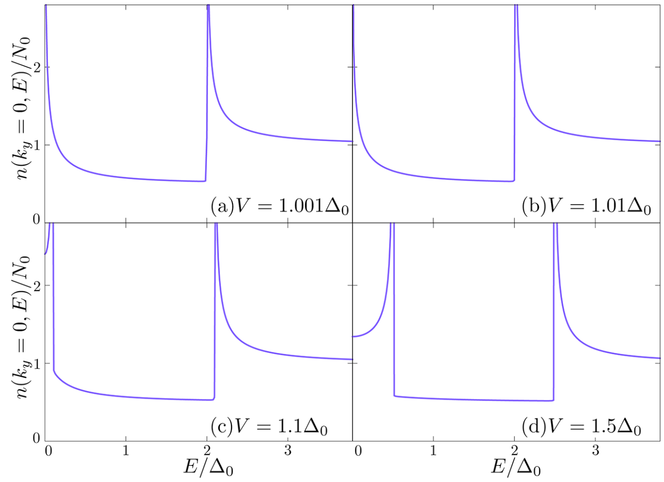

FIG. 5. The angle-resolved density of states $n(\hat{\boldsymbol{k}}, E)$ at $k_y = 0$ are shown for several Zeeman fields with $\lambda k_F = 2\Delta_0$.

as a result of the absence of the BFSs around $\boldsymbol{k} = (0, \pm k_F)$ in Fig. 2. This also explains the monotonic dependence of α^y on temperatures in Fig. 4. The BFSs spread in the k_y direction with increasing Zeeman potential as shown in Fig. 2. A quasiparticle on the BFS for $k_y \neq 0$ has a finite velocity in the y direction. Such quasiparticle states can carry the thermoelectric current in the y direction. In Fig. 2, the number of quasiparticle states for $k_y \neq 0$ increases with increasing V. As a result, α^y takes a finite value and increases even at zero temperature with increasing V. We conclude that the thermoelectric effect in a junction in Fig. 1 is remarkably anisotropic in real space because of the anisotropy of the BFSs in momentum space. The thermoelectric coefficient for the current perpendicular to a magnetic field can be larger than that in the normal state because a Zeeman potential shifts the gapped spectra in DOS depending on the spin of a quasiparticle.

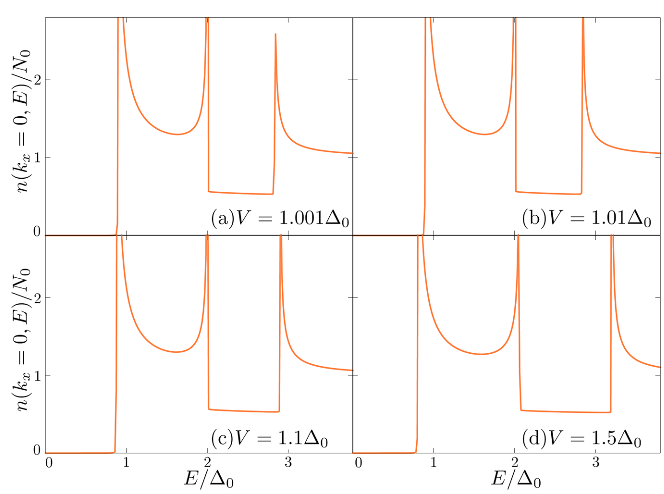

FIG. 6. The angle-resolved density of states $n(\hat{\boldsymbol{k}}, E)$ at $k_x = 0$ are shown for several Zeeman fields with $\lambda k_F = 2\Delta_0$.

V. DISCUSSION

Two of the authors have shown that odd-frequency Cooper pairs coexist with quasiparticles on the BFSs [29]. This can be seen in the expression of the anomalous Green's function in Eq. (22). The first term represents a spin-singlet Cooper pairs and is linked to the pair potential through the gap equation. The other terms represent spin-triplet Cooper pairs generated by a Zeepan potential and/or the SOI. To make discussion simpler, we put $\boldsymbol{V} = \boldsymbol{\alpha}_{\boldsymbol{k}} = 0$ at the denominator of the Green's function in Eq. (23). By applying the analytic continuation $\epsilon + i\delta \to i\omega_n$ in such a situation, the second term in Eq. (22) is relating to odd-frequency Cooper pairs because it is an odd function of the Matsubara frequency ω_n. Before calculating the thermoelectric coefficients, we had expected the contributions of odd-frequency Cooper pairs to the electric current. Therefore, we formulate the thermoelectric coefficients in terms of the Green's functions of the Gor'kov equation. In fact, the expression in Eq. (18) includes the anomalous Green's function $\hat{F}$ and $\underset{\sim}{\hat{F}}$. Unfortunately, however, we find that $\mathrm{Tr}[\hat{F}\hat{F}^\dagger - \underset{\sim}{\hat{F}}\underset{\sim}{\hat{F}}^\dagger] = 0$ for any Zeeman fields and SOIs in a spin-singlet s-wave superconductor. Only the normal Green's functions $\hat{G}$ and $\underset{\sim}{\hat{G}}$ contribute to the thermoelectric coefficient in our model. As a result, the characteristic behavior of the thermoelectric coefficients can be explained well by the residual DOS due to quasiparticles on the BFSs.

VI. CONCLUSION

We have studied the thermoelectric effect in a thin superconducting film between a conventional superconductor and an insulator. In the presence of an external magnetic field and the Rashba spin-orbit interactions, the superconducting phase having the Bogoliubov-Fermi surfaces can be realized at the thin film. The thermoelectric coefficient is calculated based on the linear response theory in the presence of the spatial gradient of a temperature. The calculated results of the thermoelectric coefficients show the remarkable anisotropy at low temperatures: the coefficient for the current perpendicular to a magnetic field is larger than that for the current parallel to a magnetic field. Moreover, the coefficient for the current perpendicular to a magnetic field can be larger than its normal state value. These characteristic features of thermoelectric effect are explained well by the anisotropy of the Bogoliubov-Fermi surfaces in momentum space. Our results indicate a way of realizing the stable Bogoliubov-Fermi surfaces and how to check the existence of the Bogoliubov-Fermi surfaces.

ACKNOWLEDGMENTS

The authors are grateful to Y. Tanaka, Y. Kawaguchi, and S. Hoshino for useful discussions. T.S. was supported by JST, the establishment of university fellowships towards the creation of science technology innovation, Grant No. JPMJFS2101. S.I. is supported by the Grant-in-Aid for Early-Career Scientists (JSPS KAKENHI Grant No. JP24K17010). S.K. was supported by JSPS KAKENHI (Grants No. JP19K14612 and No. JP22K03478) and JST CREST (Grant No. JPMJCR19T2).

APPENDIX A: FORMALISM

1. Gor'kov equation

We begin with the general expression of the electric current in terms of Keldysh Green's function,

$$G^K_{\alpha,\beta}(\mathrm{x}_1,\mathrm{x}_2) = -i\langle\psi_\alpha(\mathrm{x}_1)\psi^\dagger_\beta(\mathrm{x}_2) - \psi^\dagger_\beta(\mathrm{x}_2)\psi_\alpha(\mathrm{x}_1)\rangle, \tag{A1}$$

$$\underline{G}^K_{\alpha,\beta}(\mathrm{x}_1,\mathrm{x}_2) = -i\langle\psi^\dagger_\alpha(\mathrm{x}_1)\psi_\beta(\mathrm{x}_2) - \psi_\beta(\mathrm{x}_2)\psi^\dagger_\alpha(\mathrm{x}_1)\rangle, \tag{A2}$$

where $\mathrm{x} = (\boldsymbol{r}, t)$ is the combined representation of coordinate and $\psi_\alpha(\mathrm{x})$ $(\psi^\dagger_\alpha(\mathrm{x}))$ is the annihilation(creation) operator of an electron. By using the anticommutation relations and applying $\boldsymbol{\nabla}_{\boldsymbol{r}_1}$ from the left, the current density is expressed in terms of the Keldysh Green's function

$$\boldsymbol{j}(\mathrm{x}_1) = \frac{e\hbar}{4m}\lim_{\mathrm{x}_1\to\mathrm{x}_2}\boldsymbol{\nabla}_{\boldsymbol{r}_1}\mathrm{Tr}[\check{G}^K(\mathrm{x}_1,\mathrm{x}_2)], \tag{A3}$$

where $-e$ is the charge of an electron, Tr is the trace in spin space and particle-hole space

$$\mathrm{Tr}[\check{G}^K(\mathrm{x}_1,\mathrm{x}_2)] = \sum_\alpha\big(G^K_{\alpha,\alpha} + \underline{G}^K_{\alpha,\alpha}\big). \tag{A4}$$

The Green's function is a solution of the Gor'kov equation which describes the superconducting states

$$\int d\mathrm{x}_2\begin{bmatrix}\check{L}-\check{\Sigma}^R & -\check{\Sigma}^K\\ 0 & \check{L}-\check{\Sigma}^A\end{bmatrix}_{(\mathrm{x}_1,\mathrm{x}_2)}\begin{bmatrix}\check{G}^R & \check{G}^K\\ 0 & \check{G}^A\end{bmatrix}_{(\mathrm{x}_2,\mathrm{x}_3)} = \begin{bmatrix}\check{1} & 0\\ 0 & \check{1}\end{bmatrix}\delta(\mathrm{x}_1-\mathrm{x}_3), \tag{A5}$$

$$\check{L}(\mathrm{x}_1,\mathrm{x}_2) = i\delta(\boldsymbol{r}_1-\boldsymbol{r}_2)\partial_{t_2} - \delta(t_1-t_2)\left\{-\frac{\hbar^2}{2m}\nabla^2_{\boldsymbol{r}_2} - \mu\right\}\check{\tau}_3 - \check{V}(\mathrm{x}_1,\mathrm{x}_2), \tag{A6}$$

$$\check{V}(\mathrm{x}_1,\mathrm{x}_2) = \delta(\mathrm{x}_1-\mathrm{x}_2)\begin{bmatrix}\boldsymbol{V}\cdot\hat{\boldsymbol{\sigma}} - i\boldsymbol{\lambda}\times\hat{\boldsymbol{\nabla}}_{\boldsymbol{r}_2}\cdot\hat{\boldsymbol{\sigma}} & 0\\ 0 & -\boldsymbol{V}\cdot\hat{\boldsymbol{\sigma}}^* - i\boldsymbol{\lambda}\times\hat{\boldsymbol{\nabla}}_{\boldsymbol{r}_2}\cdot\hat{\boldsymbol{\sigma}}^*\end{bmatrix}, \tag{A7}$$

where $\check{\tau}_i (i = 1, 2, 3)$ are Pauli's matrix in particle-hole space. The self-energy consists of two contributions,

$$\check{\Sigma}^X(\mathrm{x}_1,\mathrm{x}_2) = \check{\Delta}(\mathrm{x}_1,\mathrm{x}_2) + \check{\Sigma}^X_{\mathrm{imp}}(\boldsymbol{r}_1-\boldsymbol{r}_2)\delta(t_1-t_2), \quad (X = R, A, K). \tag{A8}$$

The pair potential

$$\check{\Delta}(\mathrm{x}_1,\mathrm{x}_2) = \begin{bmatrix}0 & \hat{\Delta}(\mathrm{x}_1-\mathrm{x}_2)\\ -\hat{\Delta}^*(\mathrm{x}_1-\mathrm{x}_2) & 0\end{bmatrix}, \tag{A9}$$

is the self-energy due to the attractive interactions. The impurity self-energy is uniform in real space due to ensemble averaging and instantaneous in time.

2. Mixed representation

In what follows, we apply the mixed representation to the Green's function

$$\check{G}(\mathrm{x}_1,\mathrm{x}_2) = \check{G}(\boldsymbol{R},\boldsymbol{r},T,t) = \int\frac{d\boldsymbol{k}d\epsilon}{(2\pi)^{d+1}}\check{G}(\boldsymbol{R},\boldsymbol{k},T,\epsilon)e^{i(\boldsymbol{k}\cdot\boldsymbol{r}-\epsilon t)}, \tag{A10}$$

with

$$\boldsymbol{R} = \frac{\boldsymbol{r}_1+\boldsymbol{r}_2}{2}, \quad \boldsymbol{r} = \boldsymbol{r}_1-\boldsymbol{r}_2, \quad T = \frac{t_1+t_2}{2}, \quad t = t_1-t_2. \tag{A11}$$

The Green's function is independent of center-of-mass-time T because we consider time-independent phenomena in this paper. We have applied the Fourier transformation to the internal degree of freedom $\mathrm{x}_1 - \mathrm{x}_2$. Since $\boldsymbol{\nabla}_{\boldsymbol{r}_1} = \boldsymbol{\nabla}_{\boldsymbol{R}}/2 + \boldsymbol{\nabla}_{\boldsymbol{r}}$, we obtain

$$\boldsymbol{\nabla}_{\boldsymbol{r}_1}G(\mathrm{x}_1,\mathrm{x}_2) = \int\frac{d\boldsymbol{k}d\epsilon}{(2\pi)^{d+1}}\left[\frac{1}{2}\boldsymbol{\nabla}_{\boldsymbol{R}} + i\boldsymbol{k}\right]G(\boldsymbol{R},\boldsymbol{k},\epsilon)e^{i(\boldsymbol{k}\cdot\boldsymbol{r}-\epsilon t)}. \tag{A12}$$

In the mean-field theory of superconductivity, the spatial gradient of the Green's function is estimated as $|\boldsymbol{\nabla}_{\boldsymbol{R}}G(\boldsymbol{R},\boldsymbol{k},\epsilon)| \simeq G(\boldsymbol{R},\boldsymbol{k},\epsilon)/\xi_0$, whereas the dominant wave number to the integral is $|\boldsymbol{k}| \simeq k_F \simeq 1/\lambda_F$. The coherence length $\xi_0 = \hbar v_F/(\pi\Delta_0) \simeq$

$\epsilon_F/(\pi k_F T_c)$ is much longer than the Fermi wavelength λ_F. The first term is negligible because the transition temperature T_c is much smaller than the Fermi energy ϵ_F. By applying the argument to the current density in Eq. (A3), we obtain Eq. (6) in the text.

The derivative in $\check{L}$ is carried out as

$$\nabla_{r_2}\check{G}(\mathrm{x}_2,\mathrm{x}_3) = \int \frac{d\boldsymbol{k}d\epsilon}{(2\pi)^{d+1}}\left\{\frac{1}{2}\nabla_{\boldsymbol{R}_{23}} + \nabla_{\boldsymbol{r}_{23}}\right\}\check{G}(\boldsymbol{R}_{23},\boldsymbol{k},\epsilon)e^{i(\boldsymbol{k}\cdot\boldsymbol{r}_{23}-\epsilon t_{23})}, \tag{A13}$$

$$\simeq \int \frac{d\boldsymbol{k}d\epsilon}{(2\pi)^{d+1}} i\boldsymbol{k}\check{G}(\boldsymbol{R}_{23},\boldsymbol{k},\epsilon)e^{i(\boldsymbol{k}\cdot\boldsymbol{r}_{23}-\epsilon t_{23})}, \tag{A14}$$

$$\nabla^2_{r_2}\check{G}(\mathrm{x}_2,\mathrm{x}_3) = \int \frac{d\boldsymbol{k}d\epsilon}{(2\pi)^{d+1}}\left\{\frac{1}{4}\nabla^2_{\boldsymbol{R}_{23}} + \nabla_{\boldsymbol{R}_{23}}\cdot\nabla_{\boldsymbol{r}_{23}} + \nabla^2_{\boldsymbol{r}_{23}}\right\}\check{G}(\boldsymbol{R}_{23},\boldsymbol{k},\epsilon)e^{i(\boldsymbol{k}\cdot\boldsymbol{r}_{23}-\epsilon t_{23})},$$

$$\simeq \int \frac{d\boldsymbol{k}d\epsilon}{(2\pi)^{d+1}}\left\{i\nabla_{\boldsymbol{R}_{23}}\cdot\boldsymbol{k} - \boldsymbol{k}^2\right\}\check{G}(\boldsymbol{R}_{23},\boldsymbol{k},\epsilon)e^{i(\boldsymbol{k}\cdot\boldsymbol{r}_{23}-\epsilon t_{23})}, \tag{A15}$$

$$\partial_{t_2}\check{G}(\mathrm{x}_2,\mathrm{x}_3) = \int \frac{d\boldsymbol{k}d\epsilon}{(2\pi)^{d+1}}\left\{\frac{1}{2}\partial_{T_{23}} + \partial_{t_{23}}\right\}\check{G}(\boldsymbol{R}_{23},\boldsymbol{k},\epsilon)e^{i(\boldsymbol{k}\cdot\boldsymbol{r}_{23}-\epsilon t_{23})},$$

$$= \int \frac{d\boldsymbol{k}d\epsilon}{(2\pi)^{d+1}} i\epsilon\check{G}(\boldsymbol{R}_{23},\boldsymbol{k},\epsilon)e^{i(\boldsymbol{k}\cdot\boldsymbol{r}_{23}-\epsilon t_{23})}. \tag{A16}$$

By substituting these results into Eq. (A5), we obtain the Gor'kov equation for the mixed-representation in Eq. (7).

3. Current formula in the linear response

The spatial gradient of temperature is considered through the distribution function

$$\Phi(\epsilon,\boldsymbol{R}) = \tanh\left[\frac{\epsilon}{2T(\boldsymbol{R})}\right]. \tag{A17}$$

In what follows, we derive the current in Eq. (6) within the first order of $\nabla\Phi$. The Gor'kov equation for $\check{G}^{R,A}$ becomes

$$\left[\check{L}_0(\boldsymbol{k},\epsilon) - \check{\Sigma}^{R,A}(\boldsymbol{k},\epsilon) + \frac{i}{2}\hbar\boldsymbol{v}\cdot\nabla_{\boldsymbol{R}}\check{\tau}_3\right]\left[\check{G}_0^{R,A}(\boldsymbol{k},\epsilon) + \delta\check{G}^{R,A}(\boldsymbol{R},\boldsymbol{k},\epsilon)\right] = \check{1}, \tag{A18}$$

where $\delta\check{G}^{R,A}$ is the deviation of the Green's function from their values in equilibrium $\check{G}_0^{R,A}$. Within the first order, we obtain

$$[\check{L}_0(\boldsymbol{k},\epsilon) - \check{\Sigma}^{R,A}(\boldsymbol{k},\epsilon)]\delta\check{G}^{R,A}(\boldsymbol{R},\boldsymbol{k},\epsilon) = 0, \tag{A19}$$

because $\nabla_{\boldsymbol{R}}\check{G}_0^{R,A} = 0$ and Gor'kov equation in equilibrium $[\check{L}_0(\boldsymbol{k},\epsilon) - \check{\Sigma}^{R,A}(\boldsymbol{k},\epsilon)]\check{G}_0^{R,A}(\boldsymbol{k},\epsilon) = \check{1}$. The solution is $\delta\check{G}^{R,A}(\boldsymbol{R},\boldsymbol{k},\epsilon) = 0$. The Gor'kov equation for the Keldysh component is given in Eq. (14) We seek the solution of the form

$$\check{G}^K(\boldsymbol{R},\boldsymbol{k},\epsilon) = \check{G}_0^R(\boldsymbol{k},\epsilon)\Phi(\epsilon,\boldsymbol{R}) - \Phi(\epsilon,\boldsymbol{R})\check{G}_0^A(\boldsymbol{k},\epsilon) + \delta\check{G}^K(\boldsymbol{R},\boldsymbol{k},\epsilon), \tag{A20}$$

$$\check{\Sigma}^K(\boldsymbol{k},\epsilon) = \check{\Sigma}^R(\boldsymbol{k},\epsilon)\Phi(\epsilon,\boldsymbol{R}) - \Phi(\epsilon,\boldsymbol{R})\check{\Sigma}^A(\boldsymbol{k},\epsilon) + \delta\check{\Sigma}^K(\boldsymbol{R},\boldsymbol{k},\epsilon). \tag{A21}$$

The first term and second term in Eqs. (A20) and (A21) are the solutions in equilibrium. We put $\delta\check{\Sigma}^K = 0$ because the deviation of the self-energy $\check{\Sigma}$ is considered through the distribution function. The solution is presented in Eq. (15). By substituting the results into Eq. (6), the current density is calculated to be

$$\boldsymbol{j}^\mu(\boldsymbol{R}) = \frac{e\hbar}{8}\int\frac{d\boldsymbol{k}d\epsilon}{(2\pi)^{d+1}}\boldsymbol{v}^\mu\boldsymbol{v}^\nu\cdot\left(\nabla^\nu_{\boldsymbol{R}}\Phi\right)\mathrm{Tr}\left[\check{G}_0^R(\boldsymbol{k},\epsilon)\check{\tau}_3\left\{\check{G}_0^R(\boldsymbol{k},\epsilon) - \check{G}_0^A(\boldsymbol{k},\epsilon)\right\}\right], \tag{A22}$$

$$= -\alpha^{\mu,\nu}\nabla^\nu_{\boldsymbol{R}}T. \tag{A23}$$

The thermoelectric coefficient is given by

$$\alpha^{\mu,\nu} = \frac{e\hbar}{32\pi T^2}\int_{-\infty}^{\infty}d\epsilon\frac{\epsilon}{\cosh^2(\epsilon/2T)}\int\frac{d\boldsymbol{k}}{(2\pi)^d}\boldsymbol{v}^\mu\boldsymbol{v}^\nu I(\boldsymbol{k},\epsilon), \tag{A24}$$

$$= \frac{e\hbar}{32\pi T^2}\int_{-\infty}^{\infty}d\epsilon\frac{\epsilon}{\cosh^2(\epsilon/2T)}\int\frac{d\hat{\boldsymbol{k}}}{S_d}\hat{k}^\mu\hat{k}^\nu\int_{-\infty}^{\infty}d\xi N(\xi)v^2(\xi)I(\boldsymbol{k},\epsilon), \tag{A25}$$

$$I(\boldsymbol{k},\epsilon) \equiv \mathrm{Tr}\big[\check{G}_0^R(\boldsymbol{k},\epsilon)\check{\tau}_3\big\{\check{G}_0^R(\boldsymbol{k},\epsilon) - \check{G}_0^A(\boldsymbol{k},\epsilon)\big\}\big], \tag{A26}$$

$$= \mathrm{Tr}[\hat{G}(\hat{G}-\hat{G}^{\dagger}) - \underset{\sim}{\hat{G}}(\underset{\sim}{\hat{G}} - \underset{\sim}{\hat{G}}^{\dagger}) + \hat{F}\hat{F}^{\dagger} - \underset{\sim}{\hat{F}}\underset{\sim}{\hat{F}}^{\dagger}]^R_{(\boldsymbol{k},\epsilon)}, \tag{A27}$$

where μ and ν are respectively the direction of current density and temperature gradient. Tr in Eq. (A27) means the trace in spin space. The contribution from the anomalous Green's function vanishes by applying Tr for any Zeeman fields and spin-orbit interactions in a spin-singlet s-wave superconductor. We have used the structure of the Green's function in particle-hole space represented as

$$\check{G}^{R,A}(\boldsymbol{k},\epsilon) = \begin{bmatrix} \hat{G} & \hat{F} \\ -\underset{\sim}{\hat{F}} & -\underset{\sim}{\hat{G}} \end{bmatrix}_{(\boldsymbol{k},\epsilon)}, \quad \check{G}^A(\boldsymbol{k},\epsilon) = [\check{G}^R(\boldsymbol{k},\epsilon)]^{\dagger}. \tag{A28}$$

The thermoelectric coefficient in a spin-singlet s-wave superconductor is calculated to be

$$\alpha = \alpha_{\mathrm{N}} \frac{3}{2\pi^2} \int_{\Delta/T}^{\infty} dx \frac{x^2}{\cosh^2(x/2)}, \tag{A29}$$

$$\alpha_{\mathrm{N}} = \frac{\pi^2}{3d} e\hbar T \tau C_0, \quad C_0 = \frac{d}{d\xi} N(\xi) v^2(\xi)\bigg|_{\xi=0}, \tag{A30}$$

where τ is the relaxation time due to random impurities. The results are identical to the previous results [34]. The lower limit of integral reflects the effects of superconductivity. The thermoelectric coefficient of an s-wave superconductor is exponentially smaller than α_{N} at low temperatures $\alpha \propto \alpha_{\mathrm{N}} \exp(-\Delta/T) \ll \alpha_{\mathrm{N}}$.

APPENDIX B: ENERGY DISPERSION

In this Appendix, we discuss the role of SOI in the formation of BFSs. Figures 7(a) and 7(b) show the BFSs in momentum space at $V = 1.5\Delta_0$ calculated for $\lambda k_F = 2\Delta_0$ and $\lambda k_F = 5\Delta_0$, respectively. When λk_F increases, the outer BFSs and the inner BFSs shift the opposite direction to each other along the k_x axis. The size of the BFSs in the k_y direction is insensitive to λk_F. A direction in the two-dimensional momentum space is specified by an angle θ. The energy dispersions are plotted as a function of the wave number for several directions in momentum space. The results for $\lambda k_F = 2\Delta_0$ are displayed in Figs. 7(c)–7(e) and those for $\lambda k_F = 5\Delta_0$ are displayed in Figs. 7(f)–7(h). Comparing Figs. 7(c)–7(e) with Figs. 7(f)–7(h), the SOI shifts the energy dispersions in the k-direction, which is the main role of the SOI in the formation of BFSs. As a result, the characteristic features of the thermoelectric effect are insensitive to λk_F.

APPENDIX C: THERMOELECTRIC EFFECT IN A d-WAVE SUPERCONDUCTOR WITH BFSS

In this Appendix, we discuss the thermoelectric effect in a d-wave superconductor with the BFSs, and compare our results with the results in a normal-metal/superconductor junction [27]. The BFSs also exist by the inflation of point nodes in a d-wave superconductor in two-dimension [2]. The BdG Hamiltonian in a d-wave superconductor under a Zeeman field is represented as

$$\check{H}_{\mathrm{BdG}} = \begin{bmatrix} \hat{h}_{\mathrm{N}}(\boldsymbol{k}) & \Delta_\theta i\hat{\sigma}_y \\ -\Delta_\theta \hat{\sigma}_y & -\hat{h}_{\mathrm{N}}^*(-\boldsymbol{k}) \end{bmatrix}, \tag{C1}$$

$$\hat{h}_{\mathrm{N}} = \xi_{\boldsymbol{k}} \hat{\sigma}_0 - \boldsymbol{V} \cdot \hat{\boldsymbol{\sigma}}, \tag{C2}$$

$$\Delta_\theta = \Delta \cos[2(\theta + \beta)], \tag{C3}$$

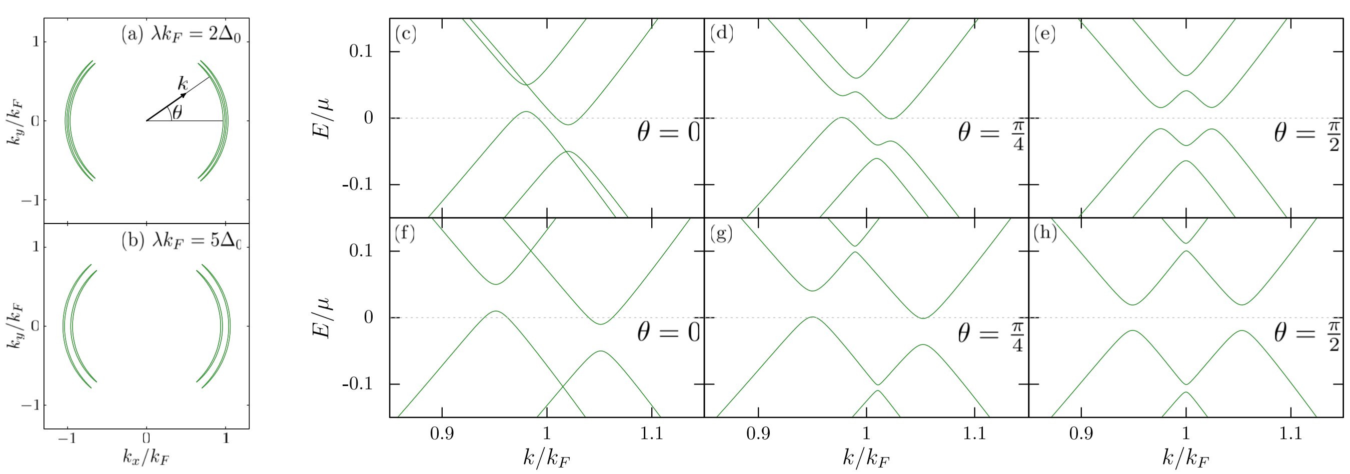

FIG. 7. The BFSs at $V = 1.5\Delta_0$ are displayed for $\lambda k_F = 2\Delta_0$ in (a) and for $\lambda k_F = 5\Delta_0$ in (b). The dispersion along several directions in momentum space are plotted for $\lambda k_F = 2\Delta_0$ in (c)–(e) and for $\lambda k_F = 5\Delta_0$ in (f)–(h). The vertical axis is normalized to the chemical potential μ.

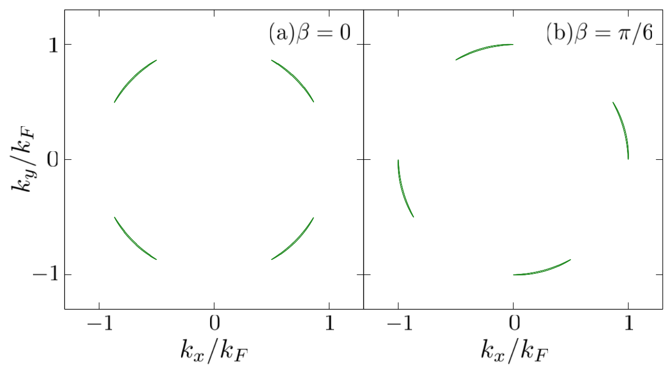

FIG. 8. The BFSs in a d-wave superconductor at $V = 0.5\Delta_0$ are displayed for $\beta = 0$ in (a) and for $\beta = \pi/6$ in (b), respectively.

with $\theta = \tan^{-1}(k_y/k_x)$ and orientation angle β, where a Zeeman field is applied in the y direction. The energy eigenvalues are calculated to be

$$E_{\boldsymbol{k}} = \sqrt{\xi_{\boldsymbol{k}}^2 + \Delta_\theta^2} \pm V, \quad -\sqrt{\xi_{\boldsymbol{k}}^2 + \Delta_\theta^2} \pm V. \tag{C4}$$

Figure 8 shows the BFSs (possible eigenvalues of the BdG Hamiltonian at zero energy) for $\beta = 0$ ($d_{x^2-y^2}$-wave) in (a) and those for $\beta = \pi/6$ in (b), where we fix a Zeeman potential at $V = 0.5\Delta_0$. The BFSs appear around the point nodes even for $V < \Delta_0$.

The DOS in a d-wave superconductor with the BFSs calculated to be

$$N(E) = \frac{N_0}{2}\int_0^{2\pi}\frac{d\theta}{2\pi}\left[\frac{|E+V|\,\Theta(|E+V| - |\Delta_\theta|)}{\sqrt{(E+V)^2 - \Delta_\theta^2}} + \frac{|E-V|\,\Theta(|E-V| - |\Delta_\theta|)}{\sqrt{(E-V)^2 - \Delta_\theta^2}}\right], \tag{C5}$$

where Θ is the step function. In Fig. 9, we present the DOS in the presence of the BFSs in a d-wave superconductor. The DOS vanishes at $E = 0$ in the absence of a Zeeman field, whereas that remains a finite value for $V = 0.5\Delta_0$.

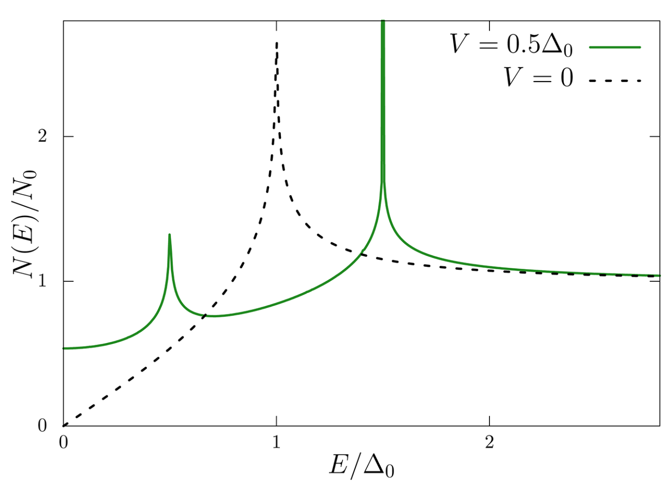

FIG. 9. The density of states (DOS) in a d-wave superconductor. The solid line shows the DOS at $V = 0.5\Delta_0$ and the dotted line shows the DOS at $V = 0$.

The shape of the pair potential on the Fermi surface is an important factor in a thermoelectric effect. Because $|\Delta_\theta| = |\Delta_{\theta+\frac{\pi}{2}}|$ holds in a d-wave superconductor, the thermoelectric coefficients in the x direction and that in the y direction are equal to each other. Therefore, we calculate the thermoelectric coefficients in the x direction α^x for several β. The thermoelectric coefficient is represented as

$$\alpha^x = \frac{e\hbar}{32\pi T^2}\int_{-\infty}^{\infty} d\epsilon \frac{\epsilon}{\cosh^2(\epsilon/2T)} \times \int_0^{2\pi}\frac{d\theta}{2\pi}\cos^2\theta \int_{-\infty}^{\infty} d\xi N(\xi)v^2(\xi)I(\xi,\theta,\epsilon). \tag{C6}$$

The results of the thermoelectric coefficients are plotted as a function of temperature in Fig. 10. The results for $V = 0$ and those for $V = 0.5\Delta_0$ are shown in Figs. 10(a) and 10(b), respectively. We assume that the dependence of Δ on temperatures is described by BCS theory and is common in Figs. 10(a) and 10(b). The solid, dashed, and dotted lines represent the coefficients for $\beta = 0$, $\beta = \pi/6$, and $\beta = \pi/4$, respectively. The numerical results indicate that the thermoelectric coefficients in a d-wave superconductor are isotropic in real space. To make this point clear, we analyze the integral of θ in Eq. (C6). As θ dependence of $I(\xi, \theta, \epsilon)$ is derived from $|\Delta_{\theta+\beta}|$ in Eq. (21), the relation

$$I(\xi,\theta,\epsilon) = I(\xi,\theta+\pi/2,\epsilon) \tag{C7}$$

holds in a d-wave superconductor even in a Zeeman field. The integral of θ is calculated to be

$$\begin{aligned}
&\int_0^{2\pi} d\theta\, \cos^2\theta\, I(\xi,\theta+\beta,\epsilon)\\
&= 2\int_0^{\pi} d\theta\, \cos^2(\theta-\beta) I(\xi,\theta,\epsilon),\\
&= 2\int_0^{\frac{\pi}{2}} d\theta\, \cos^2(\theta-\beta) I(\xi,\theta,\epsilon)\\
&\quad + 2\int_{\frac{\pi}{2}}^{\pi} d\theta\, \cos^2(\theta-\beta) I(\xi,\theta,\epsilon),\\
&= 2\int_0^{\frac{\pi}{2}} d\theta\, \cos^2(\theta-\beta) I(\xi,\theta,\epsilon)\\
&\quad + 2\int_0^{\frac{\pi}{2}} d\theta\, \cos^2(\theta-\beta+\pi/2) I(\xi,\theta+\pi/2,\epsilon),\\
&= 2\int_0^{\frac{\pi}{2}} d\theta\, \{\cos^2(\theta-\beta) + \sin^2(\theta-\beta)\} I(\xi,\theta,\epsilon),\\
&= 2\int_0^{\frac{\pi}{2}} d\theta\, I(\xi,\theta,\epsilon) \quad \text{(independent of } \beta\text{)}.
\end{aligned} \tag{C8}$$

Therefore, the thermoelectric coefficients are independent of β in a d-wave superconductor. The results also indicate $\alpha^x < \alpha_N$. To realize a large thermoelectric effect, a large Zeeman field $V \approx \Delta$ is necessary to shift the coherence peak in DOS to zero energy. However, a superconducting state becomes unstable in such large Zeeman fields.

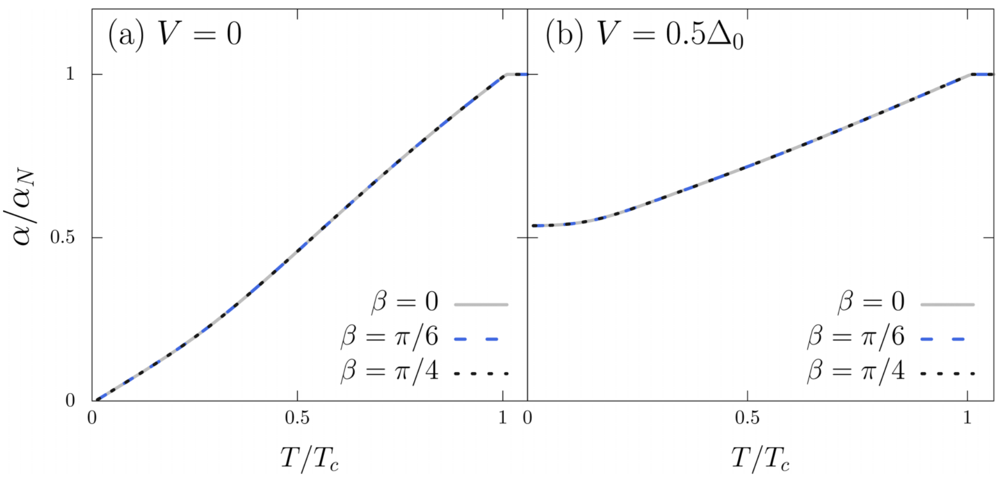

FIG. 10. The thermoelectric coefficient versus temperature in a d-wave superconductor for $V = 0$ and $V = 0.5\Delta_0$ are displayed in (a) and (b), respectively. The coefficients for $\beta = 0$, $\beta = \pi/6$, and $\beta = \pi/4$ are represented with the solid line, dashed line, and dotted line.

In a normal-metal/d-wave superconductor junction, the thermoelectric effect shows the anisotropy and the thermoelectric coefficient in a certain direction can be larger than that in the normal state. Such behaviors originate from the Andreev bound states at the interface of the junction [27].

[1] G. Volovik, Zeroes in the energy gap in superconductors with high transition temperature, Phys. Lett. A **142**, 282 (1989).
[2] K. Yang and S. L. Sondhi, Response of a $d_{x^2-y^2}$ superconductor to a Zeeman magnetic field, Phys. Rev. B **57**, 8566 (1998).
[3] D. F. Agterberg, P. M. R. Brydon, and C. Timm, Bogoliubov Fermi surfaces in superconductors with broken time-reversal symmetry, Phys. Rev. Lett. **118**, 127001 (2017).
[4] P. Burset, B. Lu, G. Tkachov, Y. Tanaka, E. M. Hankiewicz, and B. Trauzettel, Superconducting proximity effect in three-dimensional topological insulators in the presence of a magnetic field, Phys. Rev. B **92**, 205424 (2015).
[5] C. Timm, A. P. Schnyder, D. F. Agterberg, and P. M. R. Brydon, Inflated nodes and surface states in superconducting half-Heusler compounds, Phys. Rev. B **96**, 094526 (2017).
[6] T. Bzdušek and M. Sigrist, Robust doubly charged nodal lines and nodal surfaces in centrosymmetric systems, Phys. Rev. B **96**, 155105 (2017).
[7] N. F. Q. Yuan and L. Fu, Zeeman-induced gapless superconductivity with a partial Fermi surface, Phys. Rev. B **97**, 115139 (2018).
[8] P. M. R. Brydon, D. F. Agterberg, H. Menke, and C. Timm, Bogoliubov Fermi surfaces: General theory, magnetic order, and topology, Phys. Rev. B **98**, 224509 (2018).
[9] H. Menke, C. Timm, and P. M. R. Brydon, Bogoliubov Fermi surfaces stabilized by spin-orbit coupling, Phys. Rev. B **100**, 224505 (2019).
[10] J. M. Link and I. F. Herbut, Bogoliubov-Fermi surfaces in noncentrosymmetric multicomponent superconductors, Phys. Rev. Lett. **125**, 237004 (2020).
[11] C. Setty, Y. Cao, A. Kreisel, S. Bhattacharyya, and P. J. Hirschfeld, Bogoliubov Fermi surfaces in spin-$\frac{1}{2}$ systems: Model Hamiltonians and experimental consequences, Phys. Rev. B **102**, 064504 (2020).
[12] C. Timm and A. Bhattacharya, Symmetry, nodal structure, and Bogoliubov Fermi surfaces for nonlocal pairing, Phys. Rev. B **104**, 094529 (2021).
[13] S. Kobayashi, A. Bhattacharya, C. Timm, and P. M. R. Brydon, Bogoliubov Fermi surfaces from pairing of emergent $j = \frac{3}{2}$ fermions on the pyrochlore lattice, Phys. Rev. B **105**, 134507 (2022).
[14] R. Ohashi, S. Kobayashi, S. Kanazawa, Y. Tanaka, and Y. Kawaguchi, Surface density of states and tunneling spectroscopy of a spin-$\frac{3}{2}$ superconductor with Bogoliubov Fermi surfaces, Phys. Rev. B **110**, 104515 (2024).
[15] S. S. Babkin, A. P. Higginbotham, and M. Serbyn, Proximity-induced gapless superconductivity in two-dimensional Rashba semiconductor in magnetic field, SciPost Phys. **16**, 115 (2024).
[16] T. Hanaguri, K. Iwaya, Y. Kohsaka, T. Machida, T. Watashige, S. Kasahara, T. Shibauchi, and Y. Matsuda, Two distinct superconducting pairing states divided by the nematic end point in $FeSe_{1-x}S_x$, Sci. Adv. **4**, eaar6419 (2018).
[17] T. Nagashima, T. Hashimoto, S. Najafzadeh, S.-i. Ouchi, T. Suzuki, A. Fukushima, S. Kasahara, K. Matsuura, M. Qiu, Y. Mizukami, K. Hashimoto, Y. Matsuda, T. Shibauchi, S. Shin, and K. Okazaki, Discovery of nematic Bogoliubov Fermi surface in an iron-chalcogenide superconductor, Res. Sq. (2022).
[18] C. Setty, S. Bhattacharyya, Y. Cao, A. Kreisel, and P. Hirschfeld, Topological ultranodal pair states in iron-based superconductors, Nat. Commun. **11**, 523 (2020).
[19] C. J. Lapp, G. Börner, and C. Timm, Experimental consequences of Bogoliubov Fermi surfaces, Phys. Rev. B **101**, 024505 (2020).
[20] Y. Sato, S. Kasahara, T. Taniguchi, X. Xing, Y. Kasahara, Y. Tokiwa, Y. Yamakawa, H. Kontani, T. Shibauchi, and Y. Matsuda, Abrupt change of the superconducting gap structure at the nematic critical point in $FeSe_{1-x}S_x$, Proc. Natl. Acad. Sci. USA **115**, 1227 (2018).
[21] Y. Mizukami, M. Haze, O. Tanaka, K. Matsuura, D. Sano, J. Böker, I. Eremin, S. Kasahara, Y. Matsuda, and T. Shibauchi, Unusual crossover from Bardeen-Cooper-Schrieffer to Bose-

Einstein-condensate superconductivity in iron chalcogenides, Commun. Phys. **6**, 183 (2023).

[22] Z. Yu, K. Nakamura, K. Inomata, X. Shen, T. Mikuri, K. Matsuura, Y. Mizukami, S. Kasahara, Y. Matsuda, T. Shibauchi *et al.*, Spin fluctuations from Bogoliubov Fermi surfaces in the superconducting state of S-substituted FeSe, Commun. Phys. **6**, 175 (2023).

[23] T. Nagashima, K. Ishihara, K. Imamura, M. Kobayashi, M. Roppongi, K. Matsuura, Y. Mizukami, R. Grasset, M. Konczykowski, K. Hashimoto, and T. Shibauchi, Lifting of gap nodes by disorder in tetragonal $FeSe_{1-x}S_x$ superconductors, Phys. Rev. Lett. **133**, 156506 (2024).

[24] Z. Zhu, M. Papaj, X.-A. Nie, H.-K. Xu, Y.-S. Gu, X. Yang, D. Guan, S. Wang, Y. Li, C. Liu, J. Luo, Z.-A. Xu, H. Zheng, L. Fu, and J.-F. Jia, Discovery of segmented Fermi surface induced by Cooper pair momentum, Science **374**, 1381 (2021).

[25] S. Banerjee, S. Ikegaya, and A. P. Schnyder, Anomalous Fano factor as a signature of Bogoliubov Fermi surfaces, Phys. Rev. Res. **4**, L042049 (2022).

[26] J. H. Mateos, L. Tosi, A. Braggio, F. Taddei, and L. Arrachea, Nonlocal thermoelectricity in quantum wires as a signature of Bogoliubov-Fermi points, Phys. Rev. B **110**, 075415 (2024).

[27] A. Pal, P. Dutta, and A. Saha, Identifying Bogoliubov Fermi surfaces via thermoelectric response in a d-wave superconductor heterostructure, Phys. Rev. B **110**, 245417 (2024).

[28] A. Bhattacharya and C. Timm, Stability of Bogoliubov Fermi surfaces within BCS theory, Phys. Rev. B **107**, L220501 (2023).

[29] D. Kim, S. Kobayashi, and Y. Asano, Quasiparticle on Bogoliubov Fermi surface and odd-frequency Cooper pair, J. Phys. Soc. Jpn. **90**, 104708 (2021).

[30] Y. Asano and A. Sasaki, Odd-frequency Cooper pairs in two-band superconductors and their magnetic response, Phys. Rev. B **92**, 224508 (2015).

[31] T. Sato, S. Kobayashi, and Y. Asano, Discontinuous transition to a superconducting phase, Phys. Rev. B **110**, 144503 (2024).

[32] T. Miki, S.-T. Tamura, S. Iimura, and S. Hoshino, Odd-frequency pairing inherent in a Bogoliubov Fermi liquid, Phys. Rev. B **104**, 094518 (2021).

[33] Yu. M. Gal'perin, V. L. Gurevich, and V. I. Kozub, Nonlinear acoustic effects in superconductors, Zh. Eksp. Teor. Fiz. **65**, 1045 (1973).

[34] Yu. M. Galperin, V. L. Gurevich, and V. I. Kozub, Thermoelectric effects in superconductors, Zh. Eksp. Teor. Fiz. **66**, 1387 (1974).

[35] M. J. Graf, S.-K. Yip, J. A. Sauls, and D. Rainer, Electronic thermal conductivity and the Wiedemann-Franz law for unconventional superconductors, Phys. Rev. B **53**, 15147 (1996).

[36] B. S. Chandrasekhar, A note on the maximum critical field of high-field superconductors, Appl. Phys. Lett. **1**, 7 (1962).

[37] A. M. Clogston, Upper limit for the critical field in hard superconductors, Phys. Rev. Lett. **9**, 266 (1962).

[38] J. Shabani, M. Kjaergaard, H. J. Suominen, Y. Kim, F. Nichele, K. Pakrouski, T. Stankevic, R. M. Lutchyn, P. Krogstrup, R. Feidenhans'l *et al.*, Two-dimensional epitaxial superconductor-semiconductor heterostructures: A platform for topological superconducting networks, Phys. Rev. B **93**, 155402 (2016).

[39] M. Kjaergaard, F. Nichele, H. Suominen, M. Nowak, M. Wimmer, A. Akhmerov, J. Folk, K. Flensberg, J. Shabani, C. J. Palmstrøm *et al.*, Quantized conductance doubling and hard gap in a two-dimensional semiconductor–superconductor heterostructure, Nat. Commun. **7**, 12841 (2016).

[40] C. M. Moehle, C. T. Ke, Q. Wang, C. Thomas, D. Xiao, S. Karwal, M. Lodari, V. van de Kerkhof, R. Termaat, G. C. Gardner *et al.*, InSbAs two-dimensional electron gases as a platform for topological superconductivity, Nano Lett. **21**, 9990 (2021).

[41] D. Phan, J. Senior, A. Ghazaryan, M. Hatefipour, W. M. Strickland, J. Shabani, M. Serbyn, and A. P. Higginbotham, Detecting induced $p \pm ip$ pairing at the Al-InAs interface with a quantum microwave circuit, Phys. Rev. Lett. **128**, 107701 (2022).

[42] C. Reeg, D. Loss, and J. Klinovaja, Metallization of a Rashba wire by a superconducting layer in the strong-proximity regime, Phys. Rev. B **97**, 165425 (2018).